

Measurement of the Matrix Element for the Decay $\eta' \rightarrow \eta\pi^+\pi^-$

M. Ablikim¹, M. N. Achasov⁵, L. An⁹, Q. An³⁶, Z. H. An¹, J. Z. Bai¹, R. Baldini¹⁷,
 Y. Ban²³, J. Becker², N. Berger¹, M. Bertani¹⁷, J. M. Bian¹, O. Bondarenko¹⁶, I. Boyko¹⁵,
 R. A. Briere³, V. Bytev¹⁵, X. Cai¹, G. F. Cao¹, X. X. Cao¹, J. F. Chang¹, G. Chelkov^{15a},
 G. Chen¹, H. S. Chen¹, J. C. Chen¹, M. L. Chen¹, S. J. Chen²¹, Y. Chen¹, Y. B. Chen¹,
 H. P. Cheng¹¹, Y. P. Chu¹, D. Cronin-Hennessy³⁵, H. L. Dai¹, J. P. Dai¹, D. Dedovich¹⁵,
 Z. Y. Deng¹, I. Denysenko^{15b}, M. Destefanis³⁸, Y. Ding¹⁹, L. Y. Dong¹, M. Y. Dong¹, S. X. Du⁴²,
 M. Y. Duan²⁶, R. R. Fan¹, J. Fang¹, S. S. Fang¹, C. Q. Feng³⁶, C. D. Fu¹, J. L. Fu²¹, Y. Gao³²,
 C. Geng³⁶, K. Goetzen⁷, W. X. Gong¹, M. Greco³⁸, S. Grishin¹⁵, M. H. Gu¹, Y. T. Gu⁹,
 Y. H. Guan⁶, A. Q. Guo²², L. B. Guo²⁰, Y.P. Guo²², X. Q. Hao¹, F. A. Harris³⁴, K. L. He¹,
 M. He¹, Z. Y. He²², Y. K. Heng¹, Z. L. Hou¹, H. M. Hu¹, J. F. Hu⁶, T. Hu¹, B. Huang¹,
 G. M. Huang¹², J. S. Huang¹⁰, X. T. Huang²⁵, Y. P. Huang¹, T. Hussain³⁷, C. S. Ji³⁶,
 Q. Ji¹, X. B. Ji¹, X. L. Ji¹, L. K. Jia¹, L. L. Jiang¹, X. S. Jiang¹, J. B. Jiao²⁵, Z. Jiao¹¹,
 D. P. Jin¹, S. Jin¹, F. F. Jing³², M. Kavatsyuk¹⁶, S. Komamiya³¹, W. Kuehn³³, J. S. Lange³³,
 J. K. C. Leung³⁰, Cheng Li³⁶, Cui Li³⁶, D. M. Li⁴², F. Li¹, G. Li¹, H. B. Li¹, J. C. Li¹, Lei Li¹,
 N. B. Li²⁰, Q. J. Li¹, W. D. Li¹, W. G. Li¹, X. L. Li²⁵, X. N. Li¹, X. Q. Li²², X. R. Li¹, Z. B. Li²⁸,
 H. Liang³⁶, Y. F. Liang²⁷, Y. T. Liang³³, G. R. Liao⁸, X. T. Liao¹, B. J. Liu³⁰, B. J. Liu²⁹,
 C. L. Liu³, C. X. Liu¹, C. Y. Liu¹, F. H. Liu²⁶, Fang Liu¹, Feng Liu¹², G. C. Liu¹, H. Liu¹,
 H. B. Liu⁶, H. M. Liu¹, H. W. Liu¹, J. P. Liu⁴⁰, K. Liu²³, K. Y. Liu¹⁹, Q. Liu³⁴, S. B. Liu³⁶,
 X. Liu¹⁸, X. H. Liu¹, Y. B. Liu²², Y. W. Liu³⁶, Yong Liu¹, Z. A. Liu¹, Z. Q. Liu¹, H. Loehner¹⁶,
 G. R. Lu¹⁰, H. J. Lu¹¹, J. G. Lu¹, Q. W. Lu²⁶, X. R. Lu⁶, Y. P. Lu¹, C. L. Luo²⁰, M. X. Luo⁴¹,
 T. Luo¹, X. L. Luo¹, C. L. Ma⁶, F. C. Ma¹⁹, H. L. Ma¹, Q. M. Ma¹, T. Ma¹, X. Ma¹, X. Y. Ma¹,
 M. Maggiora³⁸, Q. A. Malik³⁷, H. Mao¹, Y. J. Mao²³, Z. P. Mao¹, J. G. Messchendorp¹⁶,
 J. Min¹, R. E. Mitchell¹⁴, X. H. Mo¹, N. Yu. Muchnoi⁵, Y. Nefedov¹⁵, Z. Ning¹, S. L. Olsen²⁴,
 Q. Ouyang¹, S. Pacetti¹⁷, M. Pelizaeus³⁴, K. Peters⁷, J. L. Ping²⁰, R. G. Ping¹, R. Poling³⁵,
 C. S. J. Pun³⁰, M. Qi²¹, S. Qian¹, C. F. Qiao⁶, X. S. Qin¹, J. F. Qiu¹, K. H. Rashid³⁷, G. Rong¹,
 X. D. Ruan⁹, A. Sarantsev^{15c}, J. Schulze², M. Shao³⁶, C. P. Shen³⁴, X. Y. Shen¹, H. Y. Sheng¹,
 M. R. Shepherd¹⁴, X. Y. Song¹, S. Sonoda³¹, S. Spataro³⁸, B. Spruck³³, D. H. Sun¹, G. X. Sun¹,
 J. F. Sun¹⁰, S. S. Sun¹, X. D. Sun¹, Y. J. Sun³⁶, Y. Z. Sun¹, Z. J. Sun¹, Z. T. Sun³⁶, C. J. Tang²⁷,
 X. Tang¹, X. F. Tang⁸, H. L. Tian¹, D. Toth³⁵, G. S. Varner³⁴, X. Wan¹, B. Q. Wang²³,

K. Wang¹, L. L. Wang⁴, L. S. Wang¹, M. Wang²⁵, P. Wang¹, P. L. Wang¹, Q. Wang¹,
S. G. Wang²³, X. L. Wang³⁶, Y. D. Wang³⁶, Y. F. Wang¹, Y. Q. Wang²⁵, Z. Wang¹, Z. G. Wang¹,
Z. Y. Wang¹, D. H. Wei⁸, Q.G. Wen³⁶, S. P. Wen¹, U. Wiedner², L. H. Wu¹, N. Wu¹, W. Wu¹⁹,
Z. Wu¹, Z. J. Xiao²⁰, Y. G. Xie¹, G. F. Xu¹, G. M. Xu²³, H. Xu¹, Y. Xu²², Z. R. Xu³⁶,
Z. Z. Xu³⁶, Z. Xue¹, L. Yan³⁶, W. B. Yan³⁶, Y. H. Yan¹³, H. X. Yang¹, M. Yang¹, T. Yang⁹,
Y. Yang¹², Y. X. Yang⁸, M. Ye¹, M.H. Ye⁴, B. X. Yu¹, C. X. Yu²², L. Yu¹², C. Z. Yuan¹,
W. L. Yuan²⁰, Y. Yuan¹, A. A. Zafar³⁷, A. Zallo¹⁷, Y. Zeng¹³, B. X. Zhang¹, B. Y. Zhang¹,
C. C. Zhang¹, D. H. Zhang¹, H. H. Zhang²⁸, H. Y. Zhang¹, J. Zhang²⁰, J. W. Zhang¹,
J. Y. Zhang¹, J. Z. Zhang¹, L. Zhang²¹, S. H. Zhang¹, T. R. Zhang²⁰, X. J. Zhang¹,
X. Y. Zhang²⁵, Y. Zhang¹, Y. H. Zhang¹, Z. P. Zhang³⁶, Z. Y. Zhang⁴⁰, G. Zhao¹, H. S. Zhao¹,
Jiawei Zhao³⁶, Jingwei Zhao¹, Lei Zhao³⁶, Ling Zhao¹, M. G. Zhao²², Q. Zhao¹, S. J. Zhao⁴²,
T. C. Zhao³⁹, X. H. Zhao²¹, Y. B. Zhao¹, Z. G. Zhao³⁶, Z. L. Zhao⁹, A. Zhemchugov^{15a},
B. Zheng¹, J. P. Zheng¹, Y. H. Zheng⁶, Z. P. Zheng¹, B. Zhong¹, J. Zhong², L. Zhong³²,
L. Zhou¹, X. K. Zhou⁶, X. R. Zhou³⁶, C. Zhu¹, K. Zhu¹, K. J. Zhu¹, S. H. Zhu¹, X. L. Zhu³²,
X. W. Zhu¹, Y. S. Zhu¹, Z. A. Zhu¹, J. Zhuang¹, B. S. Zou¹, J. H. Zou¹, J. X. Zuo¹, P. Zweber³⁵

(BESIII Collaboration)

¹ *Institute of High Energy Physics, Beijing 100049, P. R. China*

² *Bochum Ruhr-University, 44780 Bochum, Germany*

³ *Carnegie Mellon University, Pittsburgh, PA 15213, USA*

⁴ *China Center of Advanced Science and Technology, Beijing 100190, P. R. China*

⁵ *G.I. Budker Institute of Nuclear Physics SB RAS (BINP), Novosibirsk 630090, Russia*

⁶ *Graduate University of Chinese Academy of Sciences, Beijing 100049, P. R. China*

⁷ *GSI Helmholtzcentre for Heavy Ion Research GmbH, D-64291 Darmstadt, Germany*

⁸ *Guangxi Normal University, Guilin 541004, P. R. China*

⁹ *Guangxi University, Nanning 530004, P. R. China*

¹⁰ *Henan Normal University, Xinxiang 453007, P. R. China*

¹¹ *Huangshan College, Huangshan 245000, P. R. China*

¹² *Huazhong Normal University, Wuhan 430079, P. R. China*

¹³ *Hunan University, Changsha 410082, P. R. China*

¹⁴ *Indiana University, Bloomington, Indiana 47405, USA*

- ¹⁵ *Joint Institute for Nuclear Research, 141980 Dubna, Russia*
- ¹⁶ *KVI/University of Groningen, 9747 AA Groningen, The Netherlands*
- ¹⁷ *Laboratori Nazionali di Frascati - INFN, 00044 Frascati, Italy*
- ¹⁸ *Lanzhou University, Lanzhou 730000, P. R. China*
- ¹⁹ *Liaoning University, Shenyang 110036, P. R. China*
- ²⁰ *Nanjing Normal University, Nanjing 210046, P. R. China*
- ²¹ *Nanjing University, Nanjing 210093, P. R. China*
- ²² *Nankai University, Tianjin 300071, P. R. China*
- ²³ *Peking University, Beijing 100871, P. R. China*
- ²⁴ *Seoul National University, Seoul, 151-747 Korea*
- ²⁵ *Shandong University, Jinan 250100, P. R. China*
- ²⁶ *Shanxi University, Taiyuan 030006, P. R. China*
- ²⁷ *Sichuan University, Chengdu 610064, P. R. China*
- ²⁸ *Sun Yat-Sen University, Guangzhou 510275, P. R. China*
- ²⁹ *The Chinese University of Hong Kong, Shatin, N.T., Hong Kong.*
- ³⁰ *The University of Hong Kong, Pokfulam, Hong Kong*
- ³¹ *The University of Tokyo, Tokyo 113-0033 Japan*
- ³² *Tsinghua University, Beijing 100084, P. R. China*
- ³³ *Universitaet Giessen, 35392 Giessen, Germany*
- ³⁴ *University of Hawaii, Honolulu, Hawaii 96822, USA*
- ³⁵ *University of Minnesota, Minneapolis, MN 55455, USA*
- ³⁶ *University of Science and Technology of China, Hefei 230026, P. R. China*
- ³⁷ *University of the Punjab, Lahore-54590, Pakistan*
- ³⁸ *University of Turin and INFN, Turin, Italy*
- ³⁹ *University of Washington, Seattle, WA 98195, USA*
- ⁴⁰ *Wuhan University, Wuhan 430072, P. R. China*
- ⁴¹ *Zhejiang University, Hangzhou 310027, P. R. China*
- ⁴² *Zhengzhou University, Zhengzhou 450001, P. R. China*

^a *also at the Moscow Institute of Physics and Technology, Moscow, Russia*

^b *on leave from the Bogolyubov Institute for Theoretical Physics, Kiev, Ukraine*

c also at the PNPI, Gatchina, Russia

Abstract

The Dalitz plot of $\eta' \rightarrow \eta\pi^+\pi^-$ decay is studied using $(225.2 \pm 2.8) \times 10^6$ J/ψ events collected with the BESIII detector at the BEPCII e^+e^- collider. With the largest sample of η' decays to date, the parameters of the Dalitz plot are determined in a generalized and a linear representation. Also the branching fraction of $J/\psi \rightarrow \gamma\eta'$ is determined to be $(4.84 \pm 0.03 \pm 0.24) \times 10^{-3}$, where the first error is statistical and the second systematic.

PACS numbers: 12.39.-x, 13.25.Gv, 14.40.Be

I. INTRODUCTION

Chiral Perturbation Theory is the low energy effective theory of Quantum Chromodynamics. Below the ρ mass region, the interactions of the (π, K, η) particles are systematically analyzed within this framework. The success in the description of these low-energy interactions makes ChPT a powerful theoretical tool [1]. Although the mass of the η' is high and $\eta' \rightarrow \eta\pi^+\pi^-$ decay has a low Q value, which limit the predictive power of the Effective Chiral Lagrangian model, the experimental study of the process may supply information to test the predictions of chiral theory [2–4] and possible extensions of ChPT such as large-NC ChPT and resonance Chiral Theory [5]. The hadronic decays of the η' meson have also been extremely valuable in studies devoted to the effect of the gluon component [6] and the possible nonet of light scalars [7]. Previously, the GAMS-4 π and VES Collaborations have measured the related Dalitz plot parameters (GAMS-4 π for the $\eta' \rightarrow \eta\pi^0\pi^0$ channel [8] and VES for $\eta' \rightarrow \eta\pi^+\pi^-$ [9]) complementing older results reported by an early GAMS [10] and CLEO [11] Collaborations. In the isospin limit, the values of the Dalitz plot parameters should be the same; however the experimental measurements show some discrepancies among them.

In this article, with a new level of precision, we present results for the Dalitz plot parameters for $\eta' \rightarrow \eta\pi^+\pi^-$ based on $(225.2 \pm 2.8) \times 10^6$ J/ψ events collected by BESIII at BEPCII.

II. BESIII AND BEPCII

BESIII/BEPCII [12] is a major upgrade of the BESII experiment at the BEPC accelerator [13] for studies of hadron spectroscopy and τ -charm physics [14]. The design peak luminosity of the double-ring e^+e^- collider, BEPCII, is $10^{33} \text{ cm}^{-2}\text{s}^{-1}$ at a beam current of 0.93 A. The BESIII detector with a geometrical acceptance of 93% of 4π , consists of the following main components: 1) a small-celled, helium-based main draft chamber (MDC) with 43 layers. The average single wire resolution is 135 μm , and the momentum resolution for 1 GeV/c charged particles in a 1 T magnetic field is 0.5%; 2) an electromagnetic calorimeter (EMC) made of 6240 CsI (Tl) crystals arranged in a cylindrical shape (barrel) plus two endcaps. For 1.0 GeV photons, the energy resolution is 2.5% in the barrel and 5% in the

endcaps, and the position resolution is 6 mm in the barrel and 9 mm in the endcaps; 3) a Time-Of-Flight system (TOF) for particle identification composed of a barrel part made of two layers with 88 pieces of 5 cm thick, 2.4 m long plastic scintillators in each layer, and two endcaps with 96 fan-shaped, 5 cm thick, plastic scintillators in each endcap. The time resolution is 80 ps in the barrel, and 110 ps in the endcaps, corresponding to better than a 2 sigma K/π separation for momenta below about 1 GeV/c; 4) a muon chamber system (MUC) made of 1000 m² of Resistive Plate Chambers (RPC) arranged in 9 layers in the barrel and 8 layers in the endcaps and incorporated in the return iron of the superconducting magnet. The position resolution is about 2 cm.

The estimation of physics backgrounds are performed through Monte Carlo (MC) simulations. The GEANT4-based simulation software BOOST [15] includes the geometric and material description of the BESIII detectors, detector response and digitization models, as well as the tracking of the detector running conditions and performance. The production of the J/ψ resonance is simulated by the MC event generator KKMC [16], while the decays are generated by EvtGen [17] for known decay modes with branching fractions being set to the PDG [18] world average values, and by Lundcharm [19] for the remaining unknown decays. The analysis is performed in the framework of the BESIII Offline Software System (BOSS) [20] which takes care of the detector calibration, event reconstruction and data storage.

III. EVENT SELECTION

The η' is identified by its decay into $\eta\pi^+\pi^-$ with $\eta \rightarrow \gamma\gamma$ in J/ψ radiative decays, and candidate events with the topology $\gamma\gamma\pi^+\pi^-$ are selected using the following criteria. Charged tracks in BESIII are reconstructed from MDC hits. To optimize the momentum measurement, we select tracks in the polar angle range $|\cos\theta| < 0.93$ and require that they pass within ± 10 cm of the interaction point in the beam direction and within ± 1 cm in the plane perpendicular to the beam. Electromagnetic showers are reconstructed by clustering EMC crystal energies. Efficiency and energy resolution are improved by including energy deposits in nearby TOF counters. Showers identified as photon candidates must satisfy fiducial and shower-quality requirements. The minimum energy is 25 MeV for barrel

showers ($|\cos\theta| < 0.8$) and 50 MeV for endcap showers ($0.86 < |\cos\theta| < 0.92$). Photons in the region between the barrel and endcaps are not well measured and are not used. To exclude showers from charged particles, a photon must be separated by at least 20° from any charged track. EMC cluster timing requirements suppress electronic noise and energy deposits unrelated to the event.

The TOF (both Endcap and Barrel) and dE/dx measurements for each charged track are used to calculate $\chi_{PID}^2(i)$ values and the corresponding confidence levels $Prob_{PID}(i)$ for the hypotheses that a track is a pion, kaon, or proton, where i ($i = \pi/K/p$) is the particle type. For pion candidates, we require $Prob_{PID}(\pi) > Prob_{PID}(K)$ and $Prob_{PID}(\pi) > 0.001$.

Candidate events must have two charged tracks with zero net charge, and the number of photons should be greater than two. At least one charged track must be identified as a pion. We do four-constraint (4C) kinematic fits imposing energy and momentum conservation under the $J/\psi \rightarrow \gamma\gamma\pi^+\pi^-$ hypothesis looping over all photon candidates, and select the combination with the minimum $\chi^2(\gamma\gamma\pi^+\pi^-)$. The minimum $\chi^2(\gamma\gamma\pi^+\pi^-)$ should be less than 200, and the efficiency of this requirement is around 99%. The η candidates are selected from the combination with the two photons' invariant mass closest to η nominal mass. With the above event selections, a very clear η signal is observed. In the analysis below, we define the η signal region as $0.518 < m_{\gamma\gamma} < 0.578$ GeV/ c^2 , and the η mass sidebands region as $0.443 < m_{\gamma\gamma} < 0.473$ GeV/ c^2 or $0.623 < m_{\gamma\gamma} < 0.653$ GeV/ c^2 .

The backgrounds in the selected event sample from a number of potential background channels listed in the PDG [18] are studied with MC simulations. The background level is very low in the η' mass region. The main backgrounds are from $J/\psi \rightarrow \gamma\eta' \rightarrow \gamma\gamma\rho^0 \rightarrow \gamma\gamma\pi^+\pi^-$ and $J/\psi \rightarrow \gamma\eta' \rightarrow \gamma\gamma\omega \rightarrow \gamma\gamma\pi^+\pi^-\pi^0$, which can be described by the normalized η mass sidebands events. The other backgrounds with η candidates are from $J/\psi \rightarrow \gamma f_1(1285)/\eta(1405/1475)/f_1(1510) \rightarrow \gamma\eta\pi^+\pi^-$. None of these backgrounds give peaking backgrounds in the η' mass region. The total background contamination is estimated to be only 0.57% within the η' mass region ($\sim 3\sigma$). An inclusive MC event sample is also used to investigate other possible surviving background events, but no other possible background from the inclusive MC is found.

IV. NUMBER OF J/ψ EVENTS

The number of J/ψ events, $N_{J/\psi}$, used in this analysis is determined from the number of inclusive events. Charged tracks are selected requiring their points of closest approach to the beam line be within 15 cm of the interaction point along the beam line and within 1 cm in the plane perpendicular to the beam line, their angles with respect to the beam line, θ , must satisfy $|\cos\theta| < 0.93$, and their momenta must be less than 2.0 GeV/ c . Clusters in the EMC must have at least 25 (50) MeV of energy in the barrel (endcap) EMC, and have $|\cos\theta| < 0.93$.

Event selection requires at least two charged tracks and visible energy, E_{vis} , greater than 1.0 GeV. Here E_{vis} is defined as the sum of charged particle energies computed from the track momenta assuming pion masses, plus the neutral shower energies measured in the EMC. To reduce backgrounds from Bhabha and dimuons, events with only two charged tracks must have the momenta of the charged tracks less than 1.5 GeV/ c and their energy deposit in the EMC less than 1.0 GeV. Backgrounds from Bhabha and dimuon events surviving the selection criteria are small. The continuum contribution ($e^+e^- \rightarrow$ anything) and the surviving backgrounds are removed by subtracting the number of events selected with the above criteria from a continuum sample taken at a center of mass energy of 3.08 GeV and normalized by relative luminosity and the cross section assuming a $1/s$ dependence.

The number of J/ψ inclusive events is also determined from the distribution of \bar{z} , which is the average of the z distances from the interaction point along the beam of the point of closest approach of tracks to the beam line. Here the number of J/ψ inclusive events is taken to be the number of events in a signal region ($-4 < \bar{z} < 4$ cm) minus the number of events in sideband regions ($6 < |\bar{z}| < 10$ cm) of \bar{z} .

The efficiency is determined from data using J/ψ events from $\psi' \rightarrow \pi^+\pi^-J/\psi$ decays [21] in the BESIII 106 M ψ' sample [22]. MC simulation is used to determine a small correction (1.0108) to this efficiency arising from the two extra tracks and the motion of the J/ψ in the ψ' events. This procedure is less sensitive to differences between data and MC simulation than using only MC to determine the efficiency. The agreement between data and MC simulation is shown for the $\cos\theta$ distribution of charged tracks in Fig. 1(a) and the total energy deposit in the EMC, E_{EMC} , in Fig. 1(b). The discrepancy between data and

MC simulations in Fig. 1(b) is due to the imperfect MC generator and imperfect detector simulation. The systematic error due to the E_{mis} requirement is negligible.

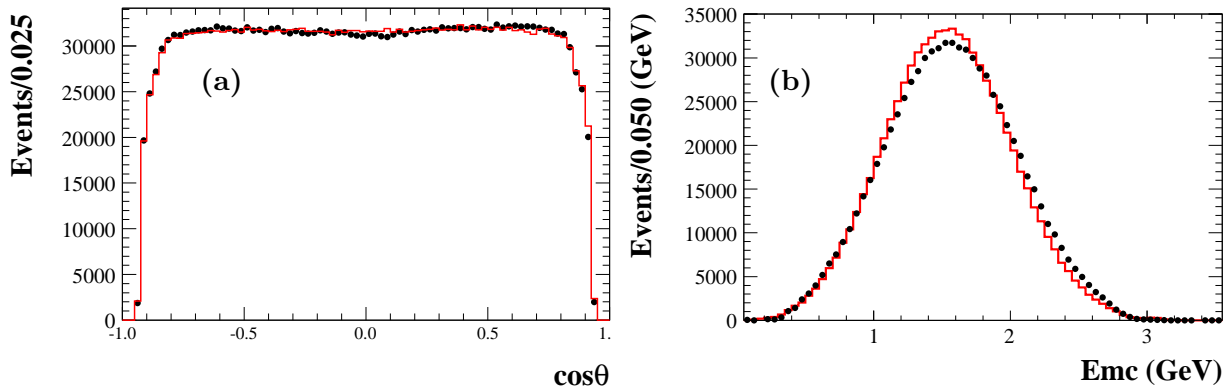


FIG. 1: (a) The $\cos\theta$ distribution of charged tracks for events satisfying selection criteria. (b) The distributions of the total energy in the EMC for events satisfying selection criteria. Dots are data, and the histogram is $J/\psi \rightarrow \text{inclusive}$ simulated events.

The result is $N_{J/\psi} = (225.2 \pm 2.8) \times 10^6$, where the error is systematic and is determined mostly by the track efficiency difference between data and MC (0.41%), the variation with the minimum charged track multiplicity requirement (0.78%), the difference when the noise levels in the two samples of J/ψ and ψ' events are modified (0.49%), the error associated with fitting the distribution of mass recoiling from the $\pi^+\pi^-$ to determine the number of $\psi' \rightarrow \pi^+\pi^- J/\psi$ events (0.45%), the error due to the continuum subtraction (0.18%), the difference between the continuum subtraction and the sideband subtraction methods for determining the number of events (0.18%), and the difference for changing the generator (0.49%). The statistical error is negligible. A second analysis determines $N_{J/\psi}$ from $J/\psi \rightarrow l^+l^-$ events, where l is a μ or e , and obtains consistent results.

V. BRANCHING FRACTION MEASUREMENT

Figure 2 shows the invariant mass distribution of $\eta\pi^+\pi^-$ candidate events. This distribution is fitted with a double-Gaussian function for the η' signal and a linear function for the background shape. The fit yields 43826 ± 211 events. The $J/\psi \rightarrow \gamma\eta'$ branching fraction is calculated using

$$\mathcal{B}(J/\psi \rightarrow \gamma\eta') = \frac{N^{obs}}{N_{J/\psi} \times \varepsilon \times \mathcal{B}(\eta' \rightarrow \eta\pi^+\pi^-) \times \mathcal{B}(\eta \rightarrow \gamma\gamma)},$$

where N^{obs} is the number of events observed, $N_{J/\psi}$ is the number of J/ψ events, and ε is the selection efficiency obtained from MC simulation, which is 23.57%. The branching fraction is then determined to be $(4.84 \pm 0.03) \times 10^{-3}$, where the error is statistical only. We also check $\mathcal{B}(J/\psi \rightarrow \gamma\eta')$ by using the number of events after the 6C kinematic fit requirement (the reconstructed momenta of two gammas are constrained to the η mass and the reconstructed momenta of $\eta\pi^+\pi^-$ is constrained to the η' mass), where the number of signal events is obtained by subtracting all the simulated normalized backgrounds with η candidates and normalized η mass sidebands events directly. The difference for $\mathcal{B}(J/\psi \rightarrow \gamma\eta')$ is only 0.3%.

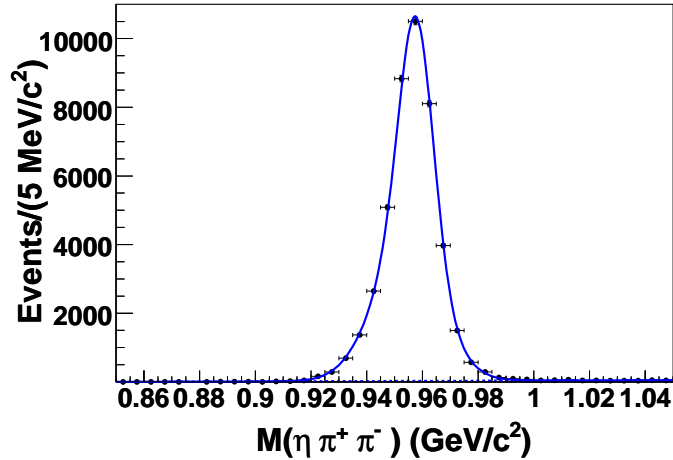


FIG. 2: The $\eta\pi^+\pi^-$ invariant mass distribution of the final candidate events. The dots with error bars represent data, and the solid curve is the result of the fit described in the text. The dashed curve is the background polynomial.

VI. MEASUREMENT OF THE MATRIX ELEMENT

The internal dynamics of the decay $\eta' \rightarrow \eta\pi^+\pi^-$ can be described by two degrees of freedom since all the particles are spin zero particles. The Dalitz plot distribution for the charged decay channel $\eta' \rightarrow \eta\pi^+\pi^-$ is described by the following two variables:

$$X = \frac{\sqrt{3}}{Q}(T_{\pi^+} - T_{\pi^-}), \quad Y = \frac{m_\eta + 2m_\pi}{m_\pi} \frac{T_\eta}{Q} - 1, \quad (1)$$

where $T_{\pi,\eta}$ denote the kinetic energies of mesons in the η' rest frame and $Q = T_\eta + T_{\pi^+} + T_{\pi^-} = m_{\eta'} - m_\eta - 2m_\pi$. The squared absolute value of the decay amplitude is expanded around the center of the corresponding Dalitz plot in order to obtain the Dalitz slope parameters:

$$M^2 = A(1 + aY + bY^2 + cX + dX^2), \quad (2)$$

where a, b, c and d are real parameters and A is a normalization factor. This parametrization is called the general decomposition. The parametrization in Eq. (2) has also been proposed with an extra term, either eXY or $fX^3 + gY^3$. For the charged channel $\eta' \rightarrow \eta\pi^+\pi^-$, odd terms in X are forbidden due to charge conjugation symmetry, while for the neutral channel $\eta' \rightarrow \eta\pi^0\pi^0$, $c = 0$ from symmetry of the wave function. The Dalitz plot parameters may not be necessarily the same for charged and neutral decay channels. However, in the isospin limit they should be the same.

A second parametrization is the linear one [18]:

$$M^2 = A(|1 + \alpha Y|^2 + cX + dX^2), \quad (3)$$

where α is a complex parameter. Of particular interest is the real component of the complex constant α , which is a linear function of the kinetic energy of the η . A non-zero value of α may represent the contribution of a gluon component in the wave function of the η' in the dynamics of its decay [10]. Comparison with the general parametrization gives $a = 2\text{Re}(\alpha)$ and $b = \text{Re}^2(\alpha) + \text{Im}^2(\alpha)$. Both parameterizations are equivalent if $b > a^2/4$.

To improve the η and η' mass resolutions and reduce the migration of events to the nearby bins in the Dalitz plot, we use kinematic information after a 6C kinematic fit to calculate the X and Y values.

Figure 3 (a) shows the experimental form of the Dalitz diagram for the decay $\eta' \rightarrow \eta\pi^+\pi^-$ in terms of the variables X and Y with the $\eta\pi^+\pi^-$ mass in the 0.93-0.98 GeV/ c^2 mass region, while the corresponding projections on variables X and Y are shown in Figs. 3 (b) and (c), respectively. In Figs. 3 (b) and (c), the dashed histograms are from MC signal sample with $\eta' \rightarrow \eta\pi^+\pi^-$ events produced with phase space, while the solid histograms are the fitted results described below. The resolutions in the variables X and Y over the entire 6C kinematical region are $\sigma_X = 0.03$ and $\sigma_Y = 0.025$, respectively, according to MC simulation.

The dependence of the matrix element on each variable, X and Y , after integration over the other, and after dividing by phase space, is shown in Fig. 4. Fitting the data with Eq. (3) gives the following values of the parameters: $\text{Re}(\alpha) = -0.035 \pm 0.005$, $\text{Im}(\alpha) = 0.00 \pm 0.08$, $c = 0.018 \pm 0.008$ and $d = -0.059 \pm 0.012$, where the errors are statistical only. Although the fitted results are consistent with world average values [18], possible correlations between the X and Y are not considered. Also the fitted value of the parameter d is not consistent

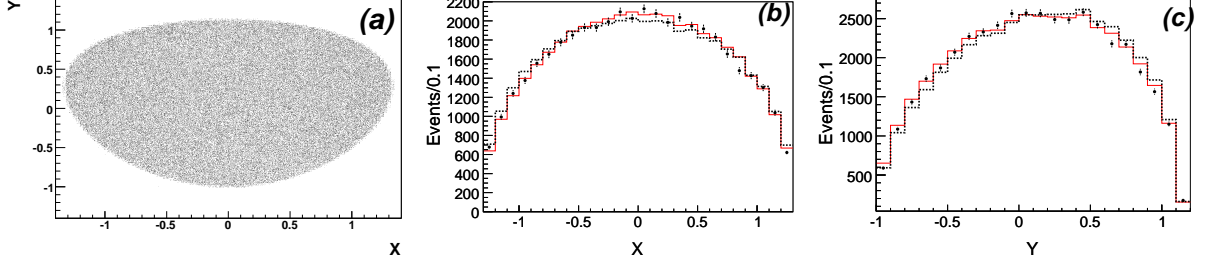


FIG. 3: (a) The experimental Dalitz diagram for the decay $\eta' \rightarrow \eta\pi^+\pi^-$ in terms of the variables X and Y with the $\eta\pi^+\pi^-$ mass in the η' mass region. The corresponding projections on variables X and Y are shown in (b) and (c), respectively, where the dashed histograms are from MC signal sample with $\eta' \rightarrow \eta\pi^+\pi^-$ events produced with phase space and the solid histograms are the fitted results described in the text.

with zero so the matrix element can not be well described by a linear function of Y only. So we do the fits to the Dalitz plot described below.

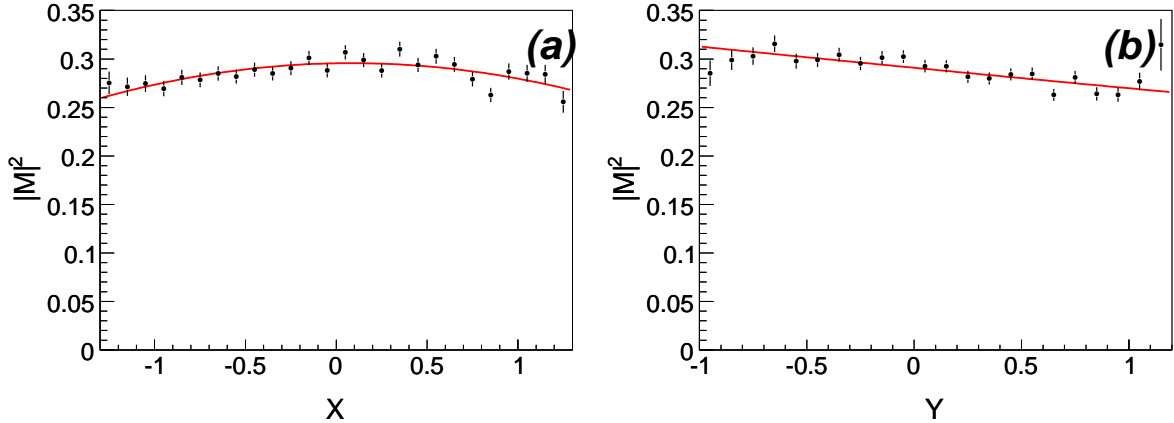


FIG. 4: Dependence of the square of the η' decay matrix element on the Dalitz variables X and Y . The solid lines are the results of the fits of the data described in the text.

In the fitting procedure, the Dalitz plot is subdivided into 26 X -bins and 22 Y -bins, i.e. 572 cells in total. Dalitz plot parameters are obtained by minimization of the function:

$$\chi^2(N, a, b, c, d) = \sum_i^{n_{bin}} \frac{(D_i - NM_i)^2}{\sigma_i^2} \quad (4)$$

Here the index i enumerates cells in Dalitz plot (empty cells outside the Dalitz plot boundaries are excluded), N is normalization factor, a, b, c and d are the Dalitz plot parameters. The M_i and D_i are the numbers of (weighted) entries in the i -th bin of the two-dimensional histograms in the Dalitz variables for MC and for the background-subtracted data, respectively. The statistical error σ includes background subtraction and MC statistical errors.

The MC histogram is obtained as follows:

$$M_i = \sum_{j=1}^{N_{ev}} (1 + aY_j + bY_j^2 + cX_j + dX_j^2), \quad (5)$$

for the general decomposition parametrization, where the index j is over the generated events and X_j and Y_j are the generated true values of Dalitz variables. Similarly for the linear parametrization,

$$M_i = \sum_{j=1}^{N_{ev}} (|1 + \alpha Y_j|^2 + cX_j + dX_j^2). \quad (6)$$

The fit procedure has been verified with MC by checking the input and output values of the Dalitz plot parameters.

First we fit using the general decomposition parametrization of the matrix element and obtain the following values for the parameters of the matrix element and for the correlation matrix ($\chi^2/NDF = 504/476$, where NDF is the number of degrees of freedom.):

$$\begin{aligned} a &= -0.047 \pm 0.011 \\ b &= -0.069 \pm 0.019 \\ c &= +0.019 \pm 0.011 \\ d &= -0.073 \pm 0.012 \end{aligned} \begin{pmatrix} 1.000 & -0.442 & -0.010 & -0.239 \\ & 1.000 & 0.025 & 0.282 \\ & & 1.000 & 0.030 \\ & & & 1.000 \end{pmatrix} \quad (7)$$

The errors are statistical only. This result is illustrated in Fig. 5, where we show the comparison of data (dots with error bars) and MC weighted with fitted coefficients (histogram) as a function of Y , in different X -intervals for $\eta' \rightarrow \eta\pi^+\pi^-$. Parameter c is consistent with zero within 1.8σ . The fitted results are almost the same with the value of parameter c fixed at zero. The statistical significance of c is estimated to be 2.1σ , from the difference of the χ^2 value taking the difference in the number of degrees of freedom ($\Delta NDF = 1$) in the fits into account.

The extra term eXY or $fX^3 + gY^3$ has also been added into the general parametrization. The fitted value of parameter e is 0.000 ± 0.018 , which is consistent with the conclusion from the VES measurement [9]. The fitted results of parameters f and g are 0.037 ± 0.035 and -0.014 ± 0.018 , respectively, and the corresponding statistical significances are very small ($\sim 1\sigma$). All the other parameter values are almost the same.

We also perform a fit using the linear parametrization of the matrix element and obtain

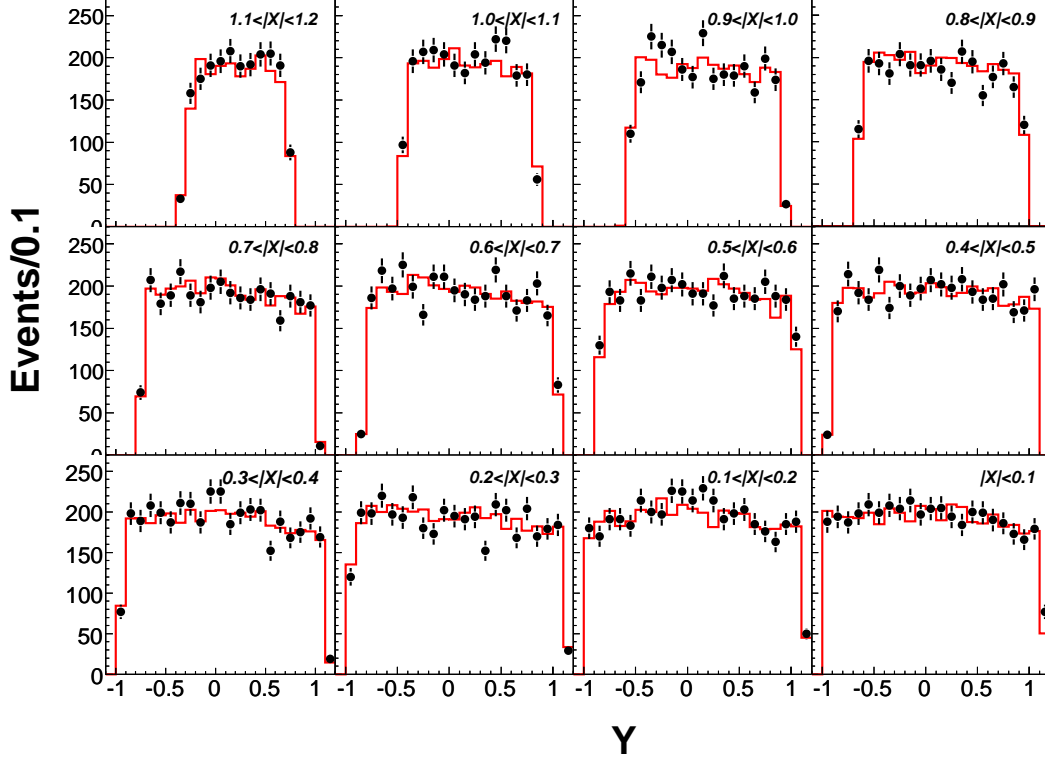


FIG. 5: Experimental distributions of the variable Y in various intervals of X with the fitting function (histogram) for the general decomposition parametrization.

($\chi^2/NDF = 521/476$):

$$\begin{aligned}
 \text{Re}(\alpha) &= -0.033 \pm 0.005 \\
 \text{Im}(\alpha) &= 0.000 \pm 0.049 \\
 c &= +0.018 \pm 0.009 \\
 d &= -0.059 \pm 0.012
 \end{aligned}
 \begin{pmatrix}
 1.000 & -0.001 & 0.001 & -0.138 \\
 & 1.000 & 0.000 & 0.000 \\
 & & 1.000 & 0.024 \\
 & & & 1.000
 \end{pmatrix}
 \quad (8)$$

The errors are statistical only. The parameter c is consistent with zero within 2.0σ , and the statistical significance is estimated to be 2.2σ .

VII. SYSTEMATIC UNCERTAINTIES

The sources of the systematic errors for the branching fraction measurement are summarized in Table I. The uncertainty is negligible for pion identification since the identification of only one of the pions is required. The uncertainty in the tracking efficiency is 1% per track and is additive. The uncertainty associated with the kinematic fit is determined to be 0.2% using the control sample $J/\psi \rightarrow \pi^+\pi^-\pi^0$. The uncertainty due to photon detection

is 1% per photon. This is determined from studies of photon detection efficiencies in well understood decays such as $J/\psi \rightarrow \rho^0\pi^0$ and study of photon conversion via $e^+e^- \rightarrow \gamma\gamma$. According to the MC simulation, the trigger efficiency for signal events is almost 100%, and the uncertainty is neglected. The background uncertainties are evaluated by changing the background fitting function from a first order polynomial to second order and the fitting range, resulting in change of the branching fraction by 0.3%. The uncertainties of $\mathcal{B}(\eta' \rightarrow \eta\pi^+\pi^-)$ and $\mathcal{B}(\eta \rightarrow \gamma\gamma)$ are 1.6% and 0.5%, respectively [18]. The fitted results to the Dalitz plot matrix element show correlations between the Dalitz plot parameters. This should be properly taken into account when integrating the amplitude over phase space to obtain the decay width. The maximum difference in the efficiency is 2.5% by using general decomposition parametrization results or linear parametrization results. The difference (2.5%) is conservatively taken into the systematic errors. Finally the uncertainty on the number of J/ψ events is 2%. Assuming that all of these systematic error sources are independent, we add them in quadrature to obtain the total systematic error shown in Table I.

TABLE I: Relative systematic errors (%) for the branching fraction measurement.

Source	$\mathcal{B}(J/\psi \rightarrow \gamma\eta')$
Part ID	—
Tracking	2.0
Kinematic fit	0.2
Photon efficiency	3.0
MC statistics	0.3
Trigger efficiency	—
Background shape	0.3
Intermediate branching fractions	1.7
Dalitz plot matrix element	2.5
Number of J/ψ events	1.3
Sum in quadrature	4.9

The systematic errors in the measurement of the Dalitz plot matrix element are summarized in Table II. The uncertainty from the backgrounds is negligible since the contamination is very small ($\sim 0.57\%$). The tracking efficiency correction functions for π^+ and π^- are ob-

tained by using the control sample $J/\psi \rightarrow \pi^+\pi^-p\bar{p}$, where the transverse momentum region of pion has covered the region of signal pion transverse momentum. The differences on the fitted values of parameters a , b , c and d are 3.3%, 3.3%, 4.4% and 1.2% in the general parametrization, and 3.3%, 4.8%, 2.4% for the parameters $\text{Re}(\alpha)$, c and d in the linear parametrization by applying the tracking efficiency correction functions for π^+ and π^- , respectively. The differences on the fitted results of parameters due to changing the $\eta\pi^+\pi^-$ mass requirement are included in the systematic errors. The fitted results are also compared using a 4C instead of the 6C kinematic fit, and the corresponding differences are taken as the systematic errors due to the kinematic fit uncertainty. Binning size was changed up to a factor of two: $0.1 < \Delta X, \Delta Y < 0.2$. The biggest differences on the fitted parameter values are taken as the systematic errors due to the binning size uncertainty. To determine the systematic errors associated with the event selection, especially for the selection of η candidates, another set of event selection criteria are applied: (1) The photon with the maximum energy is regarded as the radiative photon (γ_{rad}). (2) We do a 4C kinematic fit to the $J/\psi \rightarrow \gamma_{rad}\gamma\pi^+\pi^-$ hypothesis looping over all the other photon candidates and select the combination with the minimum $\chi^2(\gamma_{rad}\gamma\pi^+\pi^-)$. (3) The $\gamma\gamma$ mass is required to be within the η mass region. After applying the above event selection criteria, the difference on the total number of signal events is only about 0.53%. The fits to the Dalitz plot parameters are done with these events, and the differences are included into the systematic errors due to the event selection method uncertainty. The PHOTOS package [23] was used to include final state radiation (FSR). By changing the ratio of FSR events, the differences are taken into the systematic errors due to the FSR simulation uncertainty. Assuming that all the sources are independent and adding them in quadrature, one gets the total systematic errors of parameters a , b , c and d in the generalized representation are 4.9%, 12%, 12% and 3.1%, and the total systematic errors of parameters $\text{Re}(\alpha)$, c and d are 7.2%, 12% and 6.5% in the linear representation, respectively.

TABLE II: Relative errors of the parameters of the matrix element for the generalized and linear representations.

Source	generalized representation				linear representation		
	a	b	c	d	$\text{Re}(\alpha)$	c	d
Tracking efficiency	3.3	3.3	4.4	1.2	3.3	4.8	2.4
$m_{\eta\pi^+\pi^-}$ mass cut	0.9	4.8	3.3	1.7	1.4	2.1	3.2
Kinematic fit	2.8	4.9	2.1	0.7	5.2	7.0	4.7
Binning size	0.9	8.0	9.2	1.5	2.6	5.7	1.7
Different selection method	1.6	2.9	0.7	1.4	2.0	4.8	1.1
FSR simulation	1.0	0.4	1.9	0.2	0.9	0.7	0.4
Sum in quadrature	4.9	12	12	3.1	7.2	12	6.5

VIII. SUMMARY

Using the large J/ψ sample $((225.2 \pm 2.8) \times 10^6$ J/ψ events) collected with BESIII, the branching fraction of $J/\psi \rightarrow \gamma\eta'$ is measured to be

$$\mathcal{B}(J/\psi \rightarrow \gamma\eta') = (4.84 \pm 0.03 \text{ (stat)} \pm 0.24 \text{ (sys)}) \times 10^{-3},$$

which is consistent with the recent BESII value $((5.55 \pm 0.44) \times 10^{-3})$ [24] within 1.5σ , and the CLEO value $((5.24 \pm 0.17) \times 10^{-3})$ [25] within 1.4σ , which are used in obtaining the world average value $(5.28 \pm 0.15) \times 10^{-3}$ by the PDG [18].

The parameters of the matrix element for the decay process $\eta' \rightarrow \eta\pi^+\pi^-$ have been determined for the generalized and linear representations. They are:

$$a = -0.047 \pm 0.011 \pm 0.003$$

$$b = -0.069 \pm 0.019 \pm 0.009$$

$$c = +0.019 \pm 0.011 \pm 0.003$$

$$d = -0.073 \pm 0.012 \pm 0.003$$

for the generalized parametrization, and

$$\text{Re}(\alpha) = -0.033 \pm 0.005 \pm 0.003$$

$$\text{Im}(\alpha) = 0.000 \pm 0.049 \pm 0.001$$

$$c = +0.018 \pm 0.009 \pm 0.003$$

$$d = -0.059 \pm 0.012 \pm 0.004$$

for the linear parametrization, where the first errors are statistical and the second systematic.

Table III shows the experimental and theoretical values of the parameters of the matrix element squared for $\eta' \rightarrow \eta\pi^+\pi^-$ in the general parametrization (second, third and fourth columns) and in the linear parametrization (sixth, seventh and eighth columns). The theoretical values in Ref. [26] are the latest calculations within the framework of $U(3)$ chiral effective field theory in combination with a relativistic coupled-channels approach. We see: (1) The errors of our fitted parameter values are smaller compared to previous published results. (2) In the general decomposition parametrization of the matrix element, the central values of parameters a and b are consistent with the results from GAMS-4 π Collaboration [10], where the neutral decay $\eta' \rightarrow \eta\pi^0\pi^0$ events were analyzed; however the central values of parameters c and d are consistent with the results from VES Collaboration [9]. (3) The negative value of the coefficient b indicates that the two kinds of parametrization are not equivalent. This conclusion is consistent with that from GAMS-4 π Collaboration [10]; however it is different from the conclusion from the VES Collaboration [9], where the fit with linear parametrization yields an unsatisfactory $\chi^2/NDF = 170.5/114$ ratio. (4) The quadratic term in X is unambiguously different from zero. Similarly for the quadratic term in Y . The measured value of the Y -variable quadratic term (b) is not consistent with the expected value of around zero in the Effective Chiral Lagrangian model in which the lowest lying scalar meson candidates σ and κ together with the $f_0(980)$ and $a_0(980)$ are combined into a possible nonet [28]; however it can be accommodated in a $U(3)$ Chiral Unitarized model by including final state interactions [3]. The dynamical nature of this term needs further clarification. (5) The value of parameter c , which tests C parity violation in the strong interaction, is consistent with zero within 2σ in both parametrizations. In the future, with much more BESIII data, the hadronic decays of η' can be measured with higher precision, especially the Dalitz decay parameters, allowing more stringent testing of the predictions of ChPT [29].

TABLE III: Experimental and theoretical values of the parameters of the matrix element squared for $\eta' \rightarrow \eta\pi^+\pi^-$ in the general parametrization (second, third and fourth columns) and in the linear parametrization (sixth, seventh and eighth columns).

Par.	VES [9]	Theory [26]	This work	Par.	CLEO [11]	VES [27]	This work
a	-0.127 ± 0.018	-0.116 ± 0.011	-0.047 ± 0.012	Re(α)	-0.021 ± 0.025	-0.072 ± 0.014	-0.033 ± 0.006
b	-0.106 ± 0.032	-0.042 ± 0.034	-0.069 ± 0.021	Im(α)	0.000 (fixed)	0.000 ± 0.100	0.000 ± 0.050
c	$+0.015 \pm 0.018$	–	$+0.019 \pm 0.012$	c	0.000 (fixed)	$+0.020 \pm 0.019$	$+0.018 \pm 0.010$
d	-0.082 ± 0.019	$+0.010 \pm 0.019$	-0.073 ± 0.013	d	0.000 (fixed)	-0.066 ± 0.034	-0.059 ± 0.013

IX. ACKNOWLEDGMENTS

The BESIII collaboration thanks the staff of BEPCII and the computing center for their hard efforts. This work is supported in part by the Ministry of Science and Technology of China under Contract No. 2009CB825200; National Natural Science Foundation of China (NSFC) under Contracts Nos. 10625524, 10821063, 10825524, 10835001, 10935007; the Chinese Academy of Sciences (CAS) Large-Scale Scientific Facility Program; CAS under Contracts Nos. KJCX2-YW-N29, KJCX2-YW-N45; 100 Talents Program of CAS; Istituto Nazionale di Fisica Nucleare, Italy; Russian Foundation for Basic Research under Contracts Nos. 08-02-92221, 08-02-92200-NSFC-a; Siberian Branch of Russian Academy of Science, joint project No 32 with CAS; U. S. Department of Energy under Contracts Nos. DE-FG02-04ER41291, DE-FG02-91ER40682, DE-FG02-94ER40823; University of Groningen (RuG) and the Helmholtzzentrum fuer Schwerionenforschung GmbH (GSI), Darmstadt; WCU Program of National Research Foundation of Korea under Contract No. R32-2008-000-10155-0

-
- [1] A. Pich, hep-ph/9806303.
 - [2] B. Borasoy and R. Nissler, Eur. Phys. J A **26**, 383 (2005).
 - [3] N. Beisert and B. Borasoy, Nucl. Phys. A **716**, 186 (2003).
 - [4] J. Bijmens, Acta Phys. Slov. **56**, 305 (2006).
 - [5] R. Escribano, P. Masjuan and J. J. Sanz-Cillero, arXiv:1011.5884.
 - [6] S. D. Bass, Phys. Scripta T **99**, 96 (2002).

- [7] A. H. Fariborz and J. Schechter, Phys. Rev. D **60**, 034002 (1999).
- [8] A. M. Blik *et al.*, Phys. Atom. Nucl. **72**, 231 (2009).
- [9] V. Dorofeev *et al.*, Phys. Lett. B **651**, 22 (2007).
- [10] D. Alde *et al.* (LAPP Collaboration), Phys. Lett. B **177**, 115 (1986).
- [11] R. A. Briere *et al.* (CLEO Collaboration), Phys. Rev. Lett. **84**, 26 (2000).
- [12] M. Ablikim *et al.* (BES Collaboration), Nucl. Instrum. Meth. A **614**, 345 (2010).
- [13] J. Z. Bai *et al.* (BES Collaboration), Nucl. Instrum. Meth. A **344**, 319 (1994); Nucl. Instrum. Meth. A **458**, 627 (2001).
- [14] D. M. Asner *et al.*, Int. J. Mod. Phys. A **24**, No.1 (2009) supp.
- [15] Z. Y. Deng *et al.*, Chinese Physics C **30**, 371 (2006).
- [16] S. Jadach, B. F. L. Ward and Z. Was, Comp. Phys. Commu. **130**, 260 (2000); Phys. Rev. D **63**, 113009 (2001).
- [17] R. G. Ping *et al.*, Chinese Physics C **32**, 599 (2008).
- [18] K. Nakamura *et al.* (Particle Data Group), J. Phys. G **37**, 075021 (2010).
- [19] J. C. Chen, G. S. Huang, X. R. Qi, D. H. Zhang and Y. S. Zhu, Phys. Rev. D **62**, 034003 (2000).
- [20] W. D. Li *et al.*, The Offline Software for the BES-III Experiment, Proceeding of CHEP06 (Mumbai, India, 13-17 February 2006).
- [21] J. Z. Bai *et al.* (BES Collaboration), Phys. Lett. B **355**, 374 (1995) [Erratum-ibid. B **363**, 267 (1995)].
- [22] M. Ablikim *et al.* (BESIII Collaboration), Phys. Rev. D **81**, 052005 (2010).
- [23] E. Barberio and Z. Was, Comput. Phys. Commu. **79**, 291 (1994).
- [24] M. Ablikim *et al.* (BES Collaboration), Phys. Rev. D **73**, 052008 (2006).
- [25] T. K. Pedlar *et al.* (CLEO Collaboration), Phys. Rev. D **79**, 111101 (2009).
- [26] B. Borasoy and R. Nissler, Eur. Phys. J A **26**, 383 (2005).
- [27] D. V. Amelin *et al.*, Phys. Atom. Nucl. **68**, 372 (2005).
- [28] A. H. Fariborz and J. Schechter, Phys. Rev. D **60**, 034002 (1999).
- [29] Hai-Bo Li, J. Phys. G **36**, 085009 (2009).